Cognitive deficits and impaired hippocampal long-term potentiation in K_{ATP}-induced DEND syndrome

Shaul Yahil[a], David F. Wozniak[b,c], Zihan Yan[a], Steven Mennerick[b,c], and Maria S. Remedi[a,d,1]

[a]Division of Endocrinology, Metabolism, and Lipid Research, Department of Medicine, Washington University School of Medicine, St. Louis, MO 63110; [b]Department of Psychiatry, Washington University School of Medicine, St. Louis, MO 63110; [c]Taylor Family Institute for Innovative Psychiatric Research, Washington University School of Medicine, St. Louis, MO 63110; and [d]Department of Cell Biology and Physiology, Washington University School of Medicine, St. Louis, MO 63110

Edited by Lily Yeh Jan, HHMI, University of California, San Francisco, CA, and approved September 30, 2021 (received for review June 3, 2021)

ATP-sensitive potassium (K_{ATP}) gain-of-function (GOF) mutations cause neonatal diabetes, with some individuals exhibiting developmental delay, epilepsy, and neonatal diabetes (DEND) syndrome. Mice expressing K_{ATP}-GOF mutations pan-neuronally (nK_{ATP}-GOF) demonstrated sensorimotor and cognitive deficits, whereas hippocampus-specific hK_{ATP}-GOF mice exhibited mostly learning and memory deficiencies. Both nK_{ATP}-GOF and hK_{ATP}-GOF mice showed altered neuronal excitability and reduced hippocampal long-term potentiation (LTP). Sulfonylurea therapy, which inhibits K_{ATP}, mildly improved sensorimotor but not cognitive deficits in K_{ATP}-GOF mice. Mice expressing K_{ATP}-GOF mutations in pancreatic β-cells developed severe diabetes but did not show learning and memory deficits, suggesting neuronal K_{ATP}-GOF as promoting these features. These findings suggest a possible origin of cognitive dysfunction in DEND and the need for novel drugs to treat neurological features induced by neuronal K_{ATP}-GOF.

KATP | DEND | behavior | electrophysiology | cognition

ATP-sensitive potassium (K_{ATP}) channels are a unique link between cellular metabolism and membrane excitability. K_{ATP} gain-of-function (GOF) mutations have been identified as the most common cause of neonatal diabetes (1, 2), which, in many cases, manifests neurological features in a novel syndrome known as developmental delay, epilepsy, and neonatal diabetes (DEND) (3–6). Neurological symptoms of DEND include motor and developmental delays, severe epileptic phenotypes, and lifelong intellectual disabilities (7, 8). Diabetic features arise from suppression of insulin secretion by expression of K_{ATP}-GOF channels in pancreatic insulin-producing β-cells, and mice pan-neuronally expressing a DEND-associated K_{ATP}-GOF mutation showed sensorimotor deficits attributed to loss of excitability in cerebellar Purkinje neurons (9, 10). However, the involvement of K_{ATP}-GOF mutations in other neurological features as well as the treatability of these features remain unknown.

K_{ATP} channels are hetero-octameric complexes comprising four pore-forming Kir6.x and four sulfonylurea receptor subunits, with Kir6.2 and SUR1 compositions predominating in neurons of the hippocampus and cerebellum (11, 12) as well as in pancreatic insulin-producing β-cells (13). SUR1 subunits provide pharmacological sensitivity to K_{ATP} channel openers (diazoxide) and blockers (e.g., sulfonylureas such as glibenclamide and tolbutamide). Kir6.2 and SUR1 subunits each contain RKR endoplasmic reticulum retention motifs, with the expression of both subunits required to form functional channels (14). Mice globally lacking K_{ATP} demonstrate spatial learning deficits (15, 16), intrahippocampal application of the K_{ATP} channel opener diazoxide impairs spatial learning and memory (17), and intraseptal application of glibenclamide improved spatial memory defects induced by galanin or morphine in rats (18, 19). K_{ATP} currents regulate spike rates and spontaneous bursting activity in hippocampal CA1/CA3 neurons (20) and gate epileptic seizures (21), suggesting that neurological features may arise from alterations to excitability in hippocampal neurons (10). In human neonatal diabetes, sulfonylureas are effective in normalizing blood glucose (22) and often successful in restoring muscular tone, but they are not nearly as effective in treating neurological, especially cognitive, features of DEND (4, 23–25). These findings raise questions about the pathophysiology of DEND, particularly the relative contributions of neuronal and pancreatic expression of K_{ATP}-GOF channels in the development of neurological features. Here, we explored the origin, underlying mechanisms, and treatability of the cognitive deficits of DEND in mouse models expressing K_{ATP}-GOF channels in central neurons (pan-neuronal or hippocampus specific) or in pancreatic β-cells.

Results

Pan-Neuronal Expression of K_{ATP}-GOF Mutations Associates with DEND-Like Sensorimotor Deficits. To study the neurological features of DEND, we generated pan-neuronal nK_{ATP}-GOF mice (*SI Appendix*, Fig. S1). Because K_{ATP} channels require both Kir6.2 and SUR1 subunits (26), only those neurons that endogenously express SUR will form functional transgenic K_{ATP} channels (14). As expected, Kir6.2 messenger RNA (mRNA) levels were increased in nK_{ATP}-GOF mice, while SUR1 levels were unaffected (*SI Appendix*, Fig. S1 *H*, *Left*), suggesting no changes in channel density in mutant mice. Enhanced green

Significance

Gain-of-function (GOF) mutations in the ATP-sensitive potassium (K_{ATP}) channel cause neonatal diabetes, with some individuals exhibiting developmental delay, epilepsy, and neonatal diabetes (DEND) syndrome. In this study, we uncover the direct effects of neuronal expression of K_{ATP}-GOF mutations, and not diabetes per se, on the neurological features of DEND. Our results show a close link between neuronal K_{ATP}-GOF expression and cognitive dysfunction in DEND and reveal that antidiabetic sulfonylureas, which successfully treat diabetes, mitigate some sensorimotor problems but not cognitive deficits. These results have critical implications for humans, revealing the need for novel drugs to treat learning and memory deficits not only for K_{ATP}-induced DEND but also for other pathologies arising from altered ion channels in the brain.

Author contributions: S.Y., D.F.W., S.M., and M.S.R. designed research; S.Y., D.F.W., Z.Y., and M.S.R. performed research; S.Y., D.F.W., Z.Y., S.M., and M.S.R. analyzed data; S.Y. and M.S.R. wrote the paper; and D.F.W. and S.M. edited the manuscript.

The authors declare no competing interest.

This article is a PNAS Direct Submission.

[1]To whom correspondence may be addressed. Email: mremedi@wustl.edu.

This article contains supporting information online at http://www.pnas.org/lookup/suppl/doi:10.1073/pnas.2109721118/-/DCSupplemental.

Published November 3, 2021.

fluorescent protein (eGFP), coexpressed with the mutant channel, was only detected in nK_{ATP}-GOF mice (*SI Appendix*, Fig. S1 *H*, *Right*), confirming transgene expression. We verified on-target cerebellar and hippocampal recombination in nK_{ATP}-GOF mice in frozen brain slices costained with anti-GFP and anti-Cre antibodies, and we compared them to absent staining in controls (*SI Appendix*, Fig. S2 *A–C*). nK_{ATP}-GOF mice showed a significant increase in ambulatory activity [$F(1, 24) = 24.74$, $P = 0.00005$], vertical rearing frequency [$F(1, 24) = 6.354$, $P = 0.0188$], distance traveled in the periphery [$F(1, 24) = 20.71$, $P = 0.0001$] and center entries [$F(1, 24) = 13.70$, $P = 0.0011$], no differences in time spent in the center, but reduced overall resting time [(Genotype: $F(1, 24) = 17.34$, $P = 0.0003$] (Fig. 1 *A–F*). nK_{ATP}-GOF showed a significant increase in pole climb-down time [$F(1, 24) = 10.08$, $P = 0.0041$) and decreased time on the elevated ledge [$F(1, 24) = 5.653$, $P = 0.0257$] (Fig. 1 *G* and *H*). nK_{ATP}-GOF mice took significantly less time to climb to the top of a 90° screen [$F(1, 24) = 18.37$, $P = 0.0003$] (Fig. 1*I*). Although these tests predominantly reflect sensorimotor capabilities, altered emotionality and motivation in nK_{ATP}-GOF mice, as suggested by locomotor activity/sensorimotor battery tests, could result in enhanced (90° inclined screen) or decreased (e.g., pole climb-down time) performance. nK_{ATP}-GOF mice demonstrated significant deficits on the stationary [$F(1, 24) = 6.495$, $P = 0.0176$], constant speed [$F(1, 24) = 5.430$, $P = 0.0285$], and accelerating rotarod [$F(1, 24) = 6.234$, $P = 0.0198$] (Fig. 1 *J–L* and *SI Appendix*, Table S1). No significant sex effects were observed, with the exception of a significant sex-by-genotype interaction on the ledge test [$F(1, 24) = 5.086$, $P = 0.0355$] primarily driven by impaired performance in nK_{ATP}-GOF females relative to female controls (*SI Appendix*, Fig. S3*A*). Glucose tolerance tests (GTT) excluded the contribution of impaired glucose homeostasis on behavioral deficits (*SI Appendix*, Fig. S1*E*).

nK_{ATP}-GOF Mice Exhibited Some Cognitive Features of DEND. To evaluate spatial and nonspatial learning and memory, nK_{ATP}-GOF mice were tested in the Morris water maze (MWM) and Pavlovian fear conditioning. In MWM-cued trials, nK_{ATP}-GOF mice demonstrated impaired escape path length [$F(1, 24) = 10.83$, $P = 0.0031$] and latency [$F(1, 24) = 34.11$, $P = 0.00005$] and reduced swimming speeds [$F(1, 24) = 114.1$, $P = 0.00005$] (Fig. 2 *A–C*), although they showed some learning in path length [$F(1, 24 = 11.68$, $P = 0.002$] and latency [$F(1, 24 = 19.09$, $P = 0.0002$] from the first to last blocks of trials. In MWM place trials, nK_{ATP}-GOF mice demonstrated significant deficits in escape path length [$F(1, 24) = 48.91$, $P = 0.00005$], latency [$F(1, 24) = 94.60$, $P = 0.000049$], and swimming speeds [$F(1, 24) = 39.19$, $P = 0.00005$] (Fig. 2 *D–F*). In probe trials, nK_{ATP}-GOF mice demonstrated a significant reduction in platform crossing compared to controls [$F(1, 24) = 41.25$, $P = 0.00005$] (Fig. 2*G*). While controls spent more time in the target quadrant than in the other pool quadrants [$F(1, 24) = 14.6155$, $P = 0.00005$], nK_{ATP}-GOF mice spent less time in the target quadrant [$F(1, 24) = 63.57$, $P = 0.00005$) and did not show spatial bias (Fig. 2*H*).

nK_{ATP}-GOF mice exhibited similar baseline freezing levels as control mice on day 1, but when individual foot shocks (unconditioned stimulus) were paired with a tone (conditioned stimulus), they demonstrated lower freezing levels [Genotype: $F(1, 24) = 7.578$, $P = 0.0111$], although differences varied across tone–shock training (genotype-by-time interaction: [$F(2, 48) = 7.450$, $P = 0.0028$] (Fig. 2*I*). Results from the contextual fear test (day 2) showed significantly reduced freezing levels in nK_{ATP}-GOF mice [Genotype: $F(1, 24) = 7.578$, $P = 0.0111$] (Fig. 2*J*) in which differences varied across the session [genotype-by-time interaction: $F(2, 48) = 7.450$, $P = 0.0028$]. nK_{ATP}-GOF mice exhibited similar freezing levels during a 2-min altered-context baseline (day 3) and during early minutes of auditory cue testing (tone/no shock, Fig. 2*K*) but lower freezing levels for the remainder of the session [Genotype: $F(1, 24) = 28.63$, $P = 0.00005$, genotype-by-time: $F(7, 168) = 4.68$, $P = 0.0002$, genotype-by-sex: $F(1, 24) = 6.904$, $P = 0.0148$ interaction] driven by larger differences in females [$F(1, 24) = 26.16$, $P = 0.00003$] than in males [$F(1, 24) = 4.73$, $P = 0.040$] (*SI Appendix*, Fig. S3*B* and Table S2).

Hippocampal Expression of K_{ATP}-GOF Is Associated with Cognitive but Not Sensorimotor Deficits. To determine the origin of cognitive deficits in DEND syndrome, hippocampus-specific hK_{ATP}-GOF mice were run on the same assays as their nK_{ATP}-GOF counterparts. As predicted, hK_{ATP}-GOF mice showed normal GTT (*SI Appendix*, Fig. S1*F*), increased Kir6.2 mRNA levels [$t(4) = 4.088$, $P = 0.015$] but not SUR1, (*SI Appendix*, Fig. S1 *I*, *Left*), and eGFP expression in the hippocampus of transgenic mice (*SI Appendix*, Fig. S1 *I*, *Right*). We confirmed on-target recombination (*SI Appendix*, Fig. S2*B*) in the hippocampus, with no Cre or eGFP found in the cerebellum of hK_{ATP}-GOF mice. hK_{ATP}-GOF mice showed increased ambulatory activity [$F(1, 19) = 5.0704$, $P = 0.0364$] (Fig. 3*A*) and distance traveled in the periphery [$F(1, 19) = 5.322$, $P = 0.0325$] (Fig. 3*C*) but no differences in vertical rearing, center entries, time in the center, or resting time relative to controls (Fig. 3 *B* and *D–F*). hK_{ATP}-GOF mice did not show differences in any of the sensorimotor battery (Fig. 3 *G–I*) or rotarod tests (Fig. 3 *J–L* and *SI Appendix*, Table S3). In MWM-cued trials, hK_{ATP}-GOF mice showed significant deficits in escape path length [$F(1, 19) = 4.650$, $P = 0.0441$], latency [$F(1, 19) = 11.61$, $P = 0.003$], and swimming speeds [$F(1, 19) = 9.032$, $P = 0.0073$] (Fig. 4 *A–C*). They also showed significant deficits in escape latency [$F(1, 19) = 9.280$, $P = 0.0066$] and swimming speeds [$F(1, 19) = 10.18$, $P = 0.0048$] but not in path length [$F(1, 19) = 3.305$, $P = 0.0849$] in MWM place trials (Fig. 4 *D–F*). Robust differences in probe trial retention variables such as platform crossings [$F(1, 19) = 33.45$, $P = 0.00005$], time in the target quadrant [$F(1, 19) = 4.700$, $P = 0.0431$], and spatial bias were demonstrated in hK_{ATP}-GOF mice (Fig. 4 *G* and *H*). Similar baseline freezing levels were found in hK_{ATP}-GOF and control mice on day 1 of fear conditioning (Fig. 4*I*); however, hK_{ATP}-GOF mice showed significantly elevated freezing [$F(1, 19) = 9.565$, $P = 0.006$] during tone–shock training. An analysis of the contextual fear data only revealed a genotype-by-time interaction [$F(7, 133) = 2.519$, $P = 0.0360$]. Pairwise comparisons indicated similar degrees of freezing up to the middle of the test session followed by a greater habituation response in hK_{ATP}-GOF mice (Fig. 4*J*). No significant differences between groups were observed during the altered-context baseline, auditory cue test, or on shock sensitivity (Fig. 4*K* and *SI Appendix*, Table S4).

Impaired Hippocampal LTP Is Associated with Learning and Memory Deficits in K_{ATP}-GOF Induced DEND. To assess the effect of K_{ATP}-GOF mutations on neuronal excitability and synaptic function, we assayed long-term potential (LTP) induction in acute hippocampal slices. LTP induction was significantly reduced in nK_{ATP}-GOF mice relative to controls (Fig. 5*A*) with a significant difference in the simple effect of genotype [$F(1, 15) = 11.09$, $P = 0.0046$] but no genotype-by-time interaction [$F(21, 31) = 1.185$, $P = 0.2620$]. The slope of the baseline field excitatory postsynaptic potentials (fEPSP) did not differ between nK_{ATP}-GOF and littermate control mice during the pretetanic baseline (*SI Appendix*, Fig. S4*A*). Similar to nK_{ATP}-GOF mice, hK_{ATP}-GOF mice showed a significant reduction in LTP, with differences in the simple effect of genotype [$F(1, 18) = 6.518$, $P = 0.02$] (Fig. 5*B*) and genotype-by-time interaction [$F(21, 38) = 1.751$, $P = 0.0221$]. The baseline fEPSP slope did not show significant differences between hK_{ATP}-GOF and littermate control mice (*SI Appendix*, Fig. S4*B*).

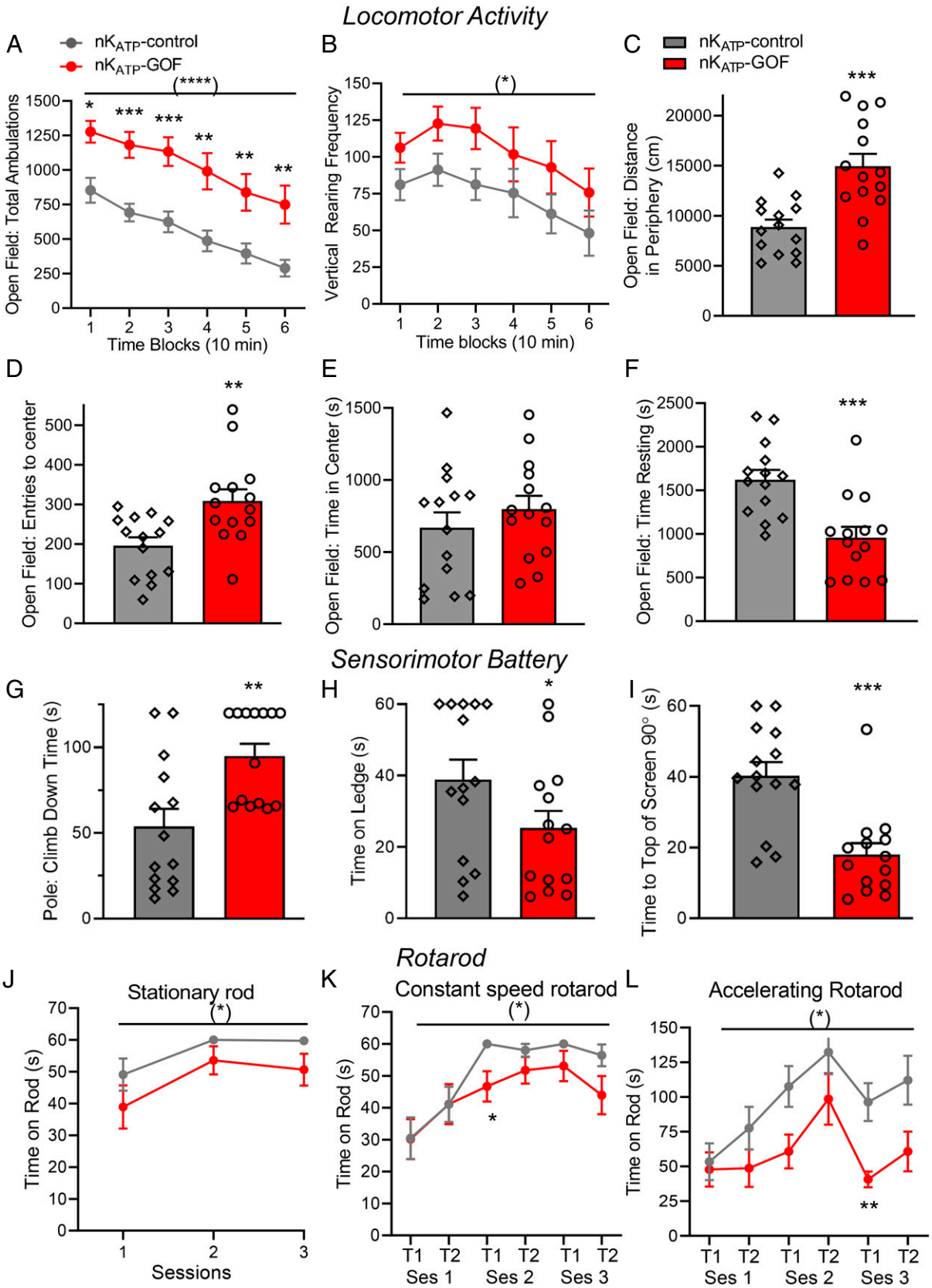

Fig. 1. Locomotor and sensorimotor functions are significantly impaired in nK$_{ATP}$-GOF mice. Locomotor activity: (*A*) total ambulations, (*B*) vertical rears, (*C*) distance traveled in the periphery, (*D*) center entries, (*E*) time in the center, and (*F*) resting time. Sensorimotor battery tests: (*G*) time to climb down pole, (*H*) time on an elevated ledge, and (*I*) time to climb to the top of 90° inclined screen. (*J*) Stationary rod, (*K*) constant speed, and (*L*) accelerating rotarod. For rotarod, T1 and T2 refer to Trials, S1 to 3 refers to Sessions. All tests shown in this figure were acquired from the same cohort. nK$_{ATP}$-GOF mice (red, $n = 14$) and littermate control mice (gray, $n = 13$). *$P < 0.05$, **$P < 0.01$, ***$P < 0.001$, ****$P < 0.0001$.

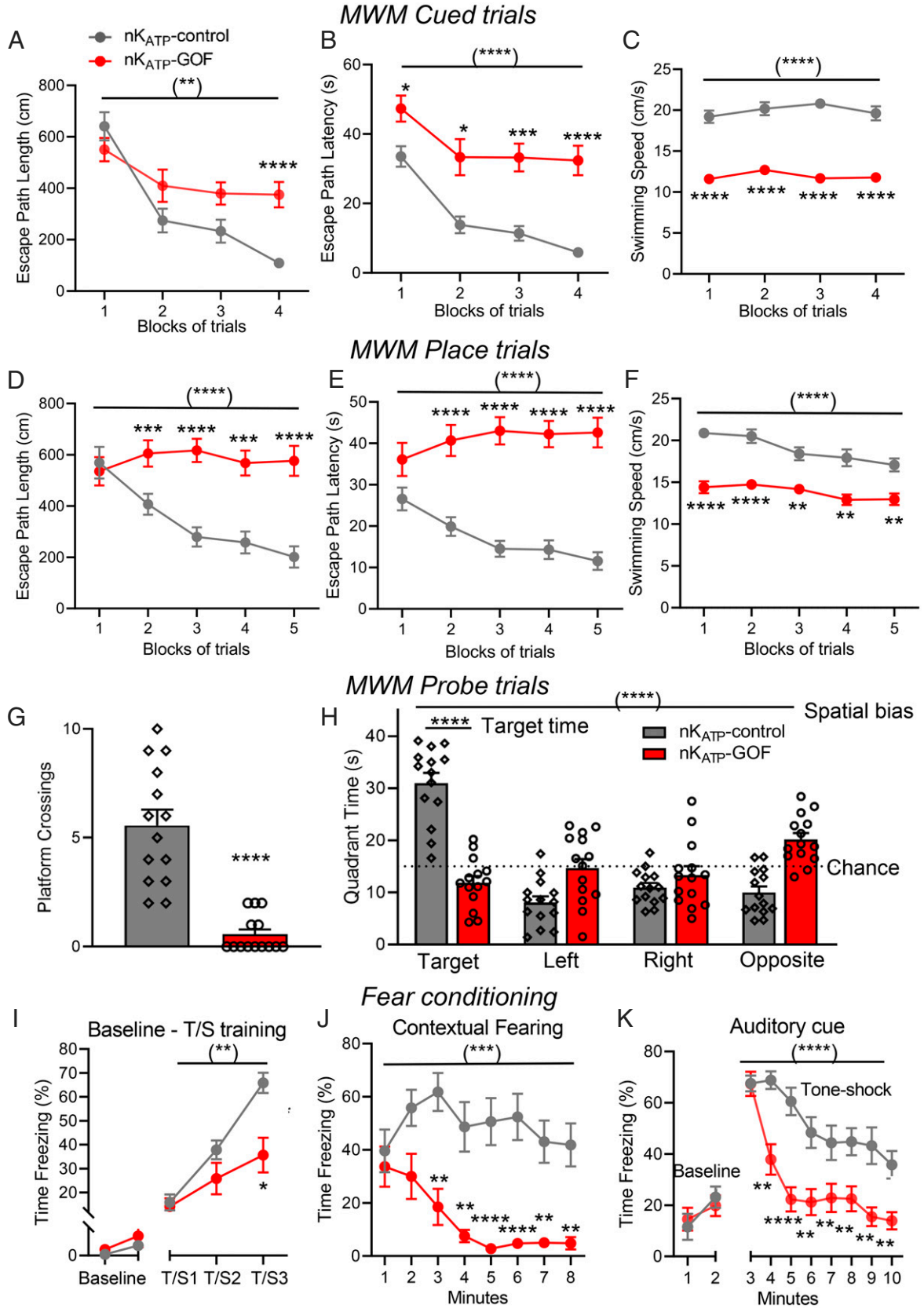

Fig. 2. MWM and fear conditioning assays reveal severe deficits in spatial learning, memory, and fear conditioning in nK_{ATP}-GOF mice in MWM-cued trials: (*A*) escape path length, (*B*) escape path latency, and (*C*) swimming speeds. MWM place trials: (*D*) escape path length, (*E*) escape path latency, and (*F*) swimming speeds. MWM probe trial: (*G*) platform crossings and (*H*) target quadrant time and spatial bias for the target quadrant. Fear conditioning: (*I*) tone–shock baseline-training, (*J*) contextual fear conditioning, and (*K*) auditory cue tests. All tests shown in this figure were acquired from the same cohort. nK_{ATP}-GOF mice (red, $n = 14$) and littermate controls (gray, $n = 13$). $^{*}P < 0.05$, $^{**}P < 0.01$, $^{***}P < 0.001$, $^{****}P < 0.0001$.

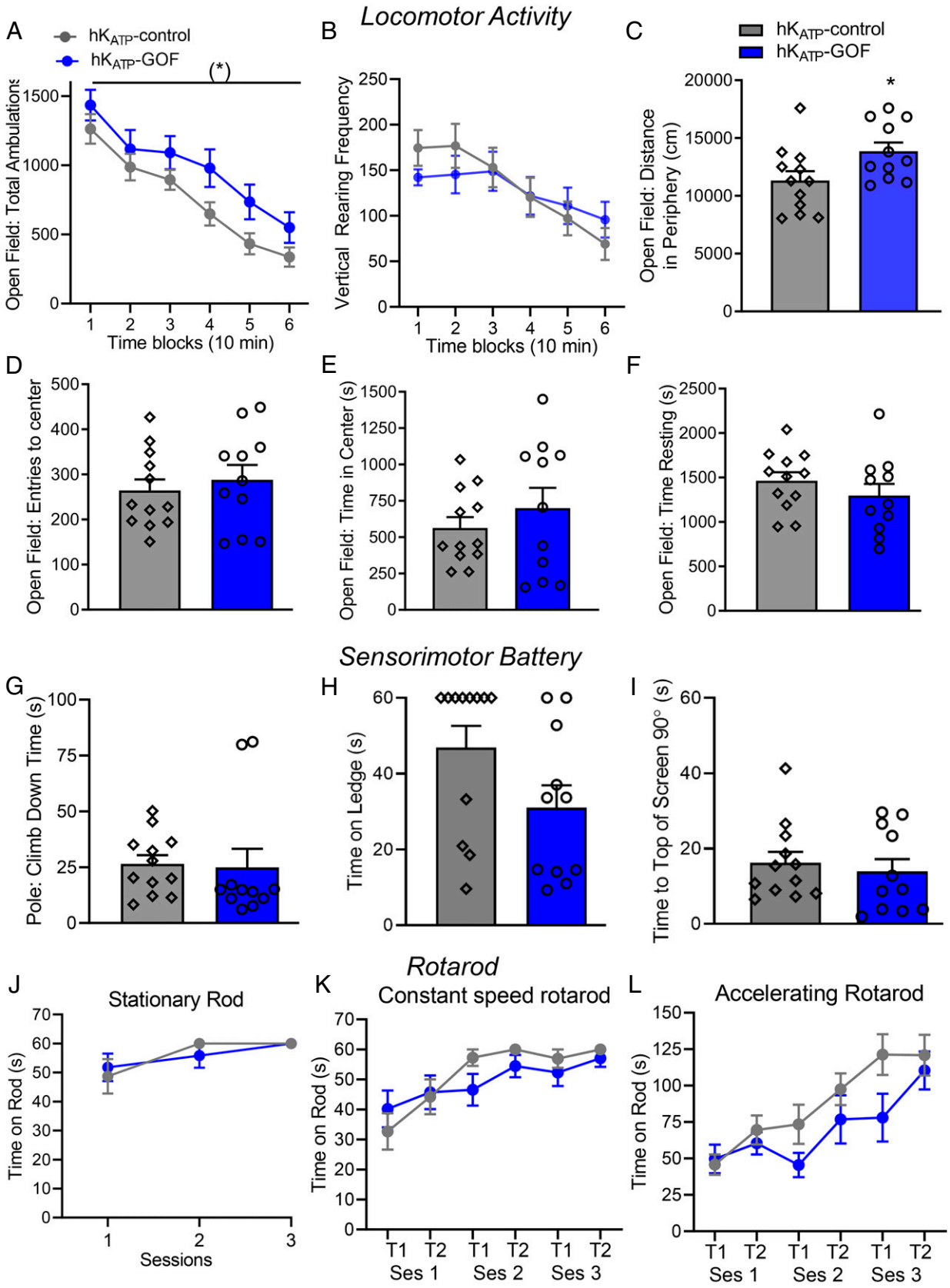

Fig. 3. Locomotor, not sensorimotor, functions are impaired in hK$_{ATP}$-GOF mice. Locomotor activity: (*A*) total ambulations, (*B*) vertical rearing, (*C*) distance in the periphery, (*D*) center entries, (*E*) time in the center, and (*F*) time resting. Sensorimotor battery: (*G*) time to climb down pole, (*H*) time on elevated ledge, and (*I*) time to climb to the top of 9° inclined screen. (*J*) Stationary rod, (*K*) constant speed, and (*L*) accelerating rotarod. All tests shown in this figure were acquired from the same cohort. hK$_{ATP}$-GOF mice (blue, $n = 12$) and controls (gray, $n = 12$). *$P < 0.05$.

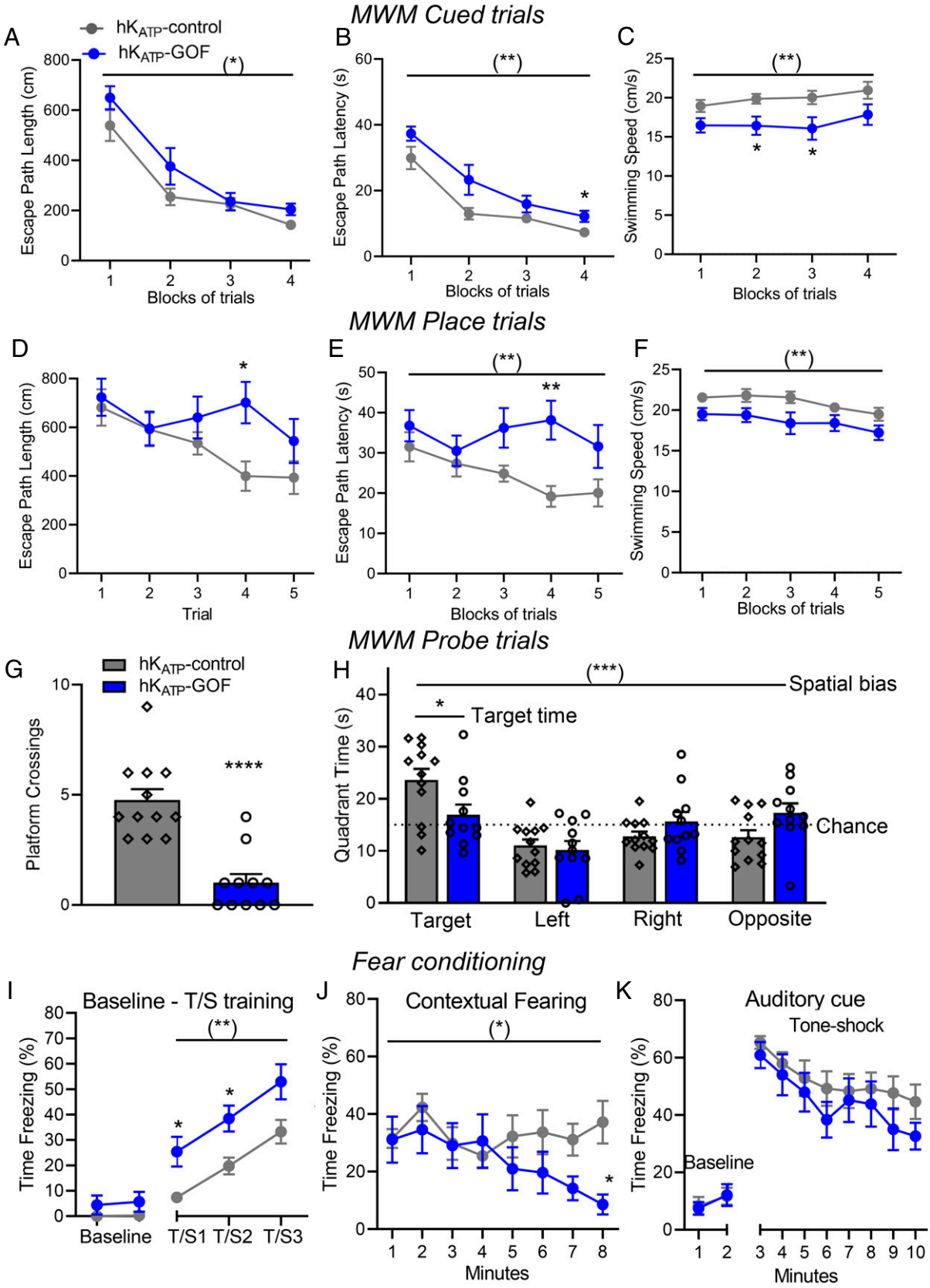

Fig. 4. MWM and fear conditioning test results reveal selective spatial learning, memory, and fear conditioning deficits in hK_{ATP}-GOF mice in MWM-cued trials: (*A*) escape path length, (*B*) latency, and (*C*) swimming speeds. MWM place trial: (*D*) escape path length, (*E*) latency, and (*F*) swimming speeds. MWM probe trial: (*G*) platform crossings and (*H*) time in the target quadrant and spatial bias for the target quadrant. Fear conditioning: (*I*) tone–shock baseline training, (*J*) contextual fear conditioning, and (*K*) auditory cue test. All tests shown in this figure were acquired from the same cohort. hK_{ATP}-GOF mice (blue, $n = 12$) and littermate controls (gray, $n = 12$). $^*P < 0.05$, $^{**}P < 0.01$, $^{***}P < 0.001$, $^{****}P < 0.0001$.

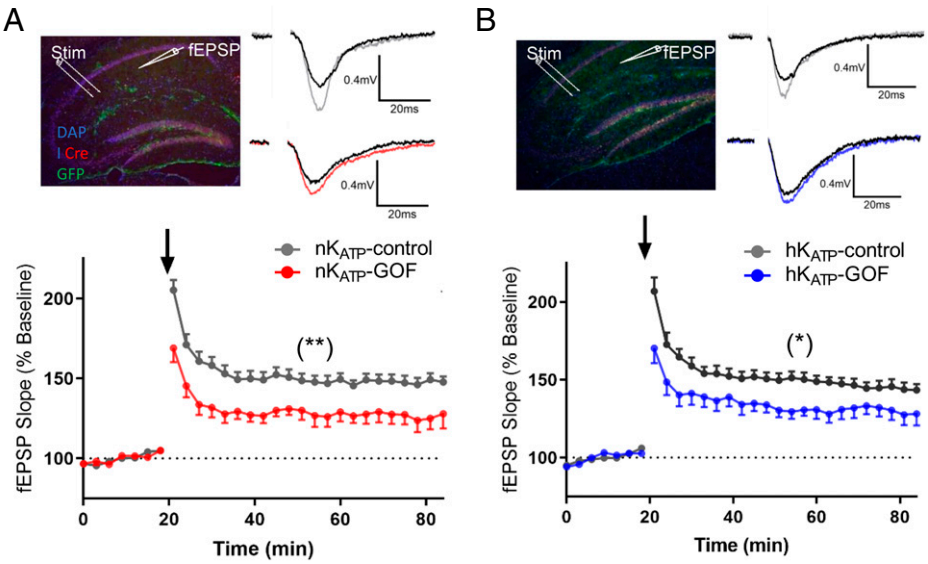

Fig. 5. nK_{ATP}-GOF mice and hK_{ATP}-GOF mice show significant changes to LTP induction. (*A*) LTP induction in hippocampal slices in nK_{ATP}-GOF mice (red, $n = 7$, 5 mice) relative to controls (gray, $n = 10$, 6 mice). (*Insets*) Representative fEPSP traces before (black) and after LTP induction in control (black to gray) and nK_{ATP}-GOF mice (black to red). (*B*) LTP induction in acute hippocampal slices in hK_{ATP}-GOF mice (blue, $n = 8$, 3 mice) and controls (gray, $n = 12$, 8 mice). (*Insets*) Representative fEPSP traces before (black) and after LTP induction in control (black to gray) and hK_{ATP}-GOF mice (black to blue). The dashed line indicates a baseline of 100% fEPSP slope. The arrow indicates the application of 100 Hz tetanus. Immunostains demonstrate representative recording locations in nK_{ATP}-GOF and hK_{ATP}-GOF frozen sections. $^*P < 0.05$, $^{**}P < 0.01$.

Hippocampal Neurons from nK_{ATP}-GOF and hK_{ATP}-GOF Mice Showed Sensitivity to K_{ATP} Channel Openers and Inhibitors. To address K_{ATP}-GOF–mediated alterations to neuronal function, whole-cell voltage ramp experiments were performed in primary cultures of dissociated hippocampal neurons. To increase the likelihood of recording K_{ATP}-specific currents and assessing K_{ATP} drug sensitivity, voltage ramps were recorded in high-potassium external solutions in the presence or absence of K_{ATP} channel openers (diazoxide) and inhibitors (tolbutamide) (Fig. 6*A*). The potential off-target effects of diazoxide were mitigated in these recordings by simultaneous application of the α-amino-3-hydroxy-5-methyl-4-isoxazolepropionic acid receptor (AMPAR) inhibitor NBQX (44). A two-way ANOVA of genotype and bath condition (Na1, K1, Dz, etc.) revealed an overall reduction in current density in nK_{ATP}-GOF mice relative to controls [genotype effect: $F(1, 24) = 7.318$, $P = 0.0124$]; however, comparisons between similar conditions (e.g., Dz-GOF to Dz-control) revealed no significant pairwise differences (Fig. 6*C*). The application of 300 μM diazoxide increased K_{ATP} current density, whereas the addition of 500 μM tolbutamide decreased it (Fig. 6*C*). The amplitude of this effect, defined as the difference in current densities between diazoxide and tolbutamide (Dz-Tol), did not differ between nK_{ATP}-GOF and control mice (Fig. 6*D*), suggesting unaffected K_{ATP} drug sensitivity in mutant mice. No significant differences in current density under any conditions were found in nK_{ATP}-GOF neurons when 0.5 mM Mg-ATP was added to the internal solution (Fig. 6*C*). hK_{ATP}-GOF neurons demonstrated no significant differences in current densities (Fig. 6*E*) or K_{ATP} drug sensitivity (Fig. 6*F*) with respect to control neurons. As predicted, neurons from global Kir6.2-knockout (K_{ATP}-KO) mice demonstrated a marked reduction in overall currents and no sensitivity to diazoxide or tolbutamide (Fig. 6*B*), confirming the specific effects of these drugs on K_{ATP}.

Learning and Memory Deficits Are Not Improved by Sulfonylurea Therapy. To test the effect of peripheral sulfonylureas on neurological features of DEND, nK_{ATP}-GOF mice were implanted with slow-release glibenclamide (Glib) pellets. Glib-nK_{ATP}-GOF mice showed significant increases in distance traveled in the periphery [$F(1, 18) = 4.644$, $P = 0.0450$] (Fig. 7*C*) and reduced time to the top of the 90° screen [$F(1, 18) = 4.593$, $P = 0.046$] (Fig. 7*F*) but no differences in total ambulations, rearing frequency, center entries (Fig. 7 *A*, *B*, and *D*), or pole climb-down time (Fig. 7*E*). Glib-nK_{ATP}-GOF mice showed no deficits in escape path length but had impaired latency [$F(1, 18) = 7.137$, $P = 0.0156$] and swimming speeds [$F(1, 18) = 12.71$, $P = 0.0022$] during MWMcued trials (Fig. 6 *G*–*I*) and impaired escape path length [$F(1, 18) = 20.01$, $P = 0.0003$], latency [$F(1, 18) = 36.68$, $P < 0.00005$], and swimming speeds [$F(1, 18) = 11.29$, $P = 0.0035$] during place trials (Fig. 7 *J*–*L*). Glib-nK_{ATP}-GOF mice showed reduced platform crossings [$F(1, 18) = 21.94$, $P = 0.0002$] and time in target quadrant [$F(1, 18) = 38.87$, $P = 0.00005$] and no spatial bias during probe trials (Fig. 7 *M* and *N*). During fear conditioning, Glib-nK_{ATP}-GOF mice exhibited similar baseline freezing levels on day 1 but lower freezing levels during certain training trials [$F(1, 18) = 4.768$, $P = 0.0425$, genotype-by-time interaction: $F(2, 36) = 4.525$, $P = 0.0188$] (Fig. 7*O*). Contextual conditioning was still significantly impaired in Glib-nK_{ATP}-GOF mice [$F(1, 18) = 20.69$, $P = 0.0002$] (Fig. 7*P*). No significant differences were observed during the altered-context baseline, but Glib-nK_{ATP}-GOF mice demonstrated significantly lower freezing levels on average across minutes during the auditory cue test [$F(1, 18) = 7.567$, $P = 0.0131$] (Fig. 7*Q* and *SI Appendix*, Table S5).

Severely Diabetic βK_{ATP}-GOF Mice Did Not Demonstrate Cognitive Deficits. To test if diabetes contributes to the neurological features of DEND, pancreatic β-cell–specific K_{ATP}-GOF mice (*SI Appendix*, Fig. S1*G*) (9) were assayed on behavioral tests. βK_{ATP}-GOF mice displayed reduced ambulations [$F(1, 18) = 6.845$, $P = 0.0175$] and distance traveled in the periphery [$F(1, 18) = 9.048$, $P = 0.0076$] and increased resting time [$F(1, 20) = 2.770$, $P = 0.0188$] (*SI Appendix*, Fig. S5 *A*, *C*, and *E*) with no differences in vertical rearing or center entries (*SI Appendix*, Fig. S5 *B* and *D*). Sensorimotor battery tests showed a significant increase in the time to climb to the top of 60° [$F(1, 18) = 8.274$, $P = 0.0100$] and 90° screens [$F(1, 18) = 6.570$, $P = 0.0196$] (*SI Appendix*,

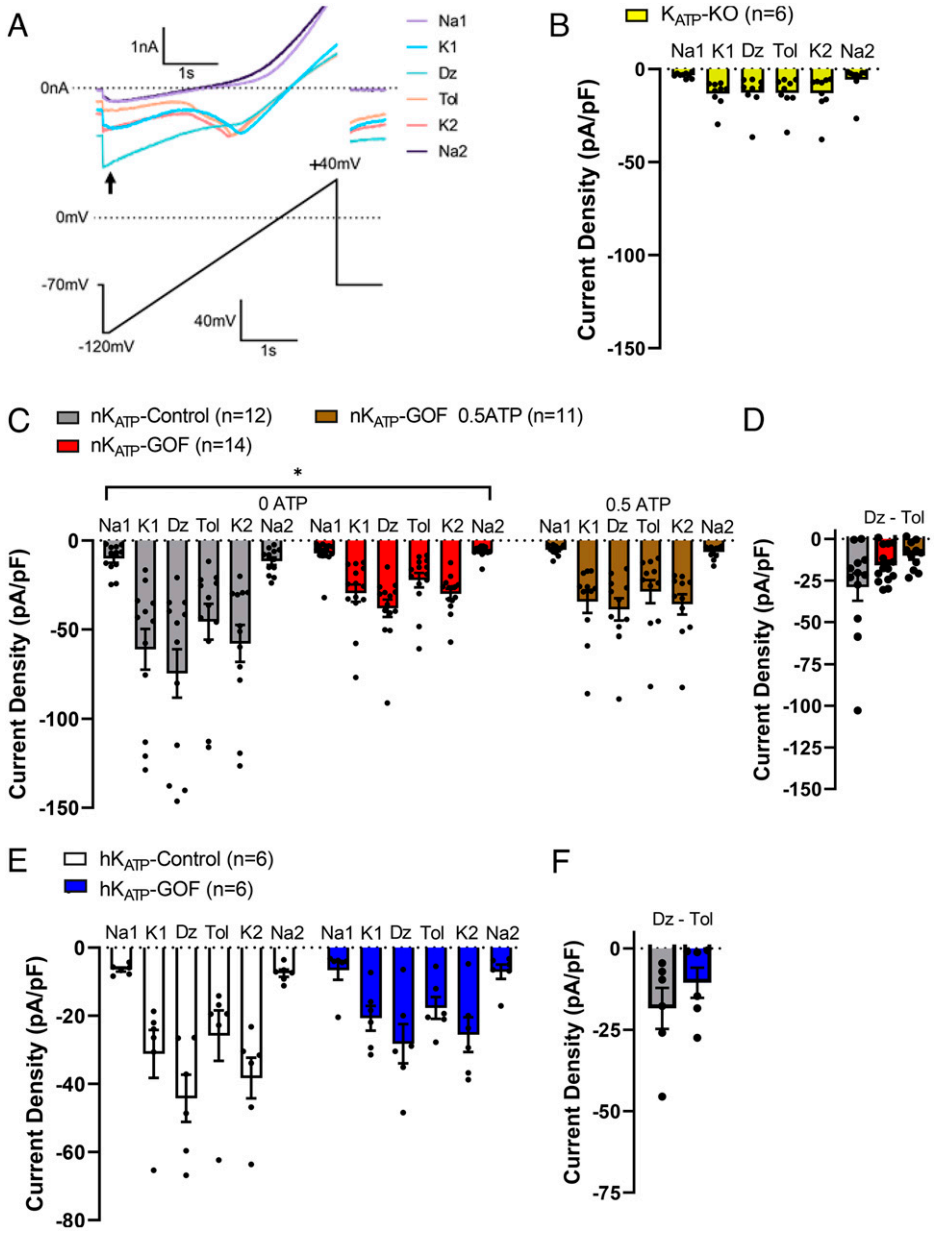

Fig. 6. Current densities in dissociated hippocampal neurons from nK_{ATP}-GOF and hK_{ATP}-GOF mice. (*A*) Representative trace of voltage ramp protocol from control neuron, from low potassium (Na1) to high-potassium (K1), to high-potassium with 300 μM Dz, to high-potassium with 500 μM Tol, high-potassium (K2), to low-potassium (Na2). (*Lower*) Schematic of the voltage ramp protocol used. The arrow indicates the point at which the current was measured and analyzed, −120 mV after 10 ms settling. (*B*) Hippocampal neurons recorded from Kir6.2-KO mice (yellow, $n = 6$). (*C*) Hippocampal neurons from nK_{ATP}-GOF mice (red, $n = 14$) and littermate controls (gray, $n = 12$). Current densities in nK_{ATP}-GOF mice were recorded with 0 mM Mg-ATP- (red) or 0.5 mM Mg-ATP-internal solutions (brown, $n = 11$). *(D)* Drug sensitivity was measured by subtracting Dz from Tol current densities (Dz-Tol) for each genotype in *(C)*. (*E*) Hippocampal neurons from hK_{ATP}-GOF mice (blue, $n = 6$) and littermate controls (white, $n = 6$). (*F*) Drug sensitivity (Dz-Tol) for data in *(E)* is shown. Statistical significance was assayed with two-way (2 × 6 genotype-by-bath condition) ANOVA with pairwise post-hoc comparisons in which $*P < 0.05$ represents a significant main effect. Nonsignificant differences are not indicated.

Fig. S5 *F* and *G*) but no differences in time on ledge, pole climb-down time, or time on inverted screen (*SI Appendix*, Fig. S5 *H*, *I*, and *J*). βK_{ATP}-GOF mice did not exhibit performance deficits on MWM-cued or place trials (*SI Appendix*, Fig. S5 *K–N*). βK_{ATP}-GOF mice showed a significant decrease in platform crossing [$F(1, 18) = 13.05$, $P = 0.0020$] (*SI Appendix*, Fig. S5*O*) but no differences in time in the target quadrant and no evidence of spatial bias in probe trials (*SI Appendix*, Fig. S5*P*). βK_{ATP}-GOF mice did not show differences in freezing during baseline or tone/shock training on day 1 (*SI Appendix*, Fig. S5*Q*) but significantly increased freezing [genotype-by-time interaction, $F(7, 126) = 3.060$, $P = 0.0100$] during certain minutes of contextual fear conditioning (*SI Appendix*, Fig. S5*R*). βK_{ATP}-GOF mice showed variably increased altered-context baseline freezing [genotype-by-time interaction, $F(7, 126) = 7.224$, $P = 0.0150$] but no differences during the actual auditory cue test (*SI Appendix*, Fig. S5*S* and Table S6).

Discussion

K_{ATP}-GOF–activating mutations are the most common cause of neonatal diabetes and are associated with DEND syndrome

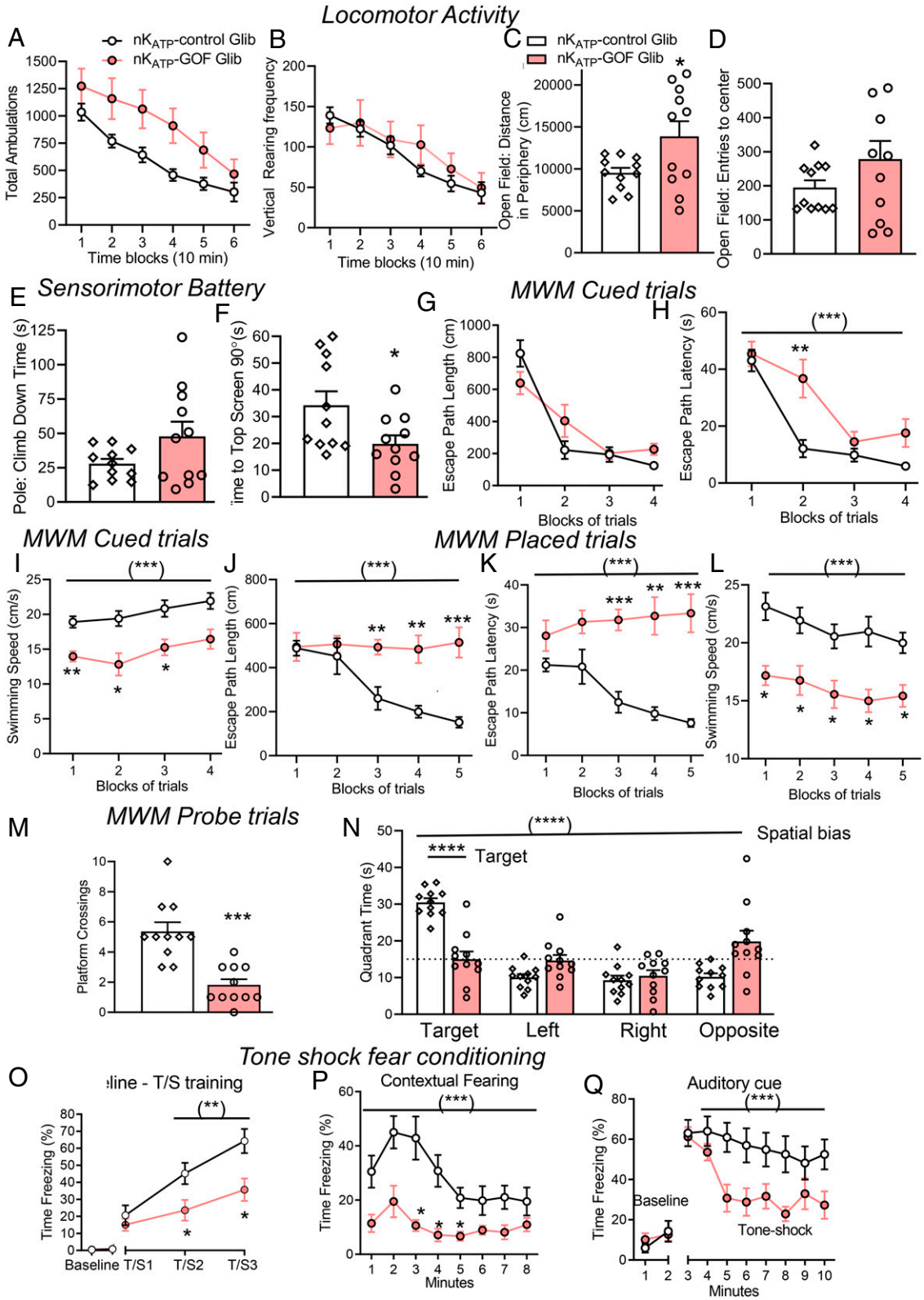

Fig. 7. Glib therapy selectively improves locomotor and sensorimotor, not neurological, features of DEND. Locomotor activity: (*A*) total ambulations, (*B*) vertical rearings, (*C*) distance traveled in the periphery, and (*D*) center entries in Glib-nK$_{ATP}$-GOF (pink, $n = 11$) and littermate controls (white, $n = 11$). Sensorimotor battery: (*E*) pole climb-down time and (*F*) time to the top of a 90° inclined screen. MWM-cued trials: (*G*) escape path length, (*H*) escape path latency, and (*I*) swimming speeds. MWM place trials: (*J*) escape path length, (*K*) escape path latency, and (*L*) swimming speeds. MWM probe trial: (*M*) platform crossings and (*N*) time in the target quadrant and spatial bias. Glib-nK$_{ATP}$ control mice demonstrated spatial bias for the target quadrant by spending significantly more time in it versus the other pool quadrants (all *P*s < 0.0001), but Glib-nK$_{ATP}$-GOF did not demonstrate a similar bias. Fear conditioning: (*O*) tone–shock baseline training, (*P*) contextual fear, and (*Q*) auditory cue tests. *$P < 0.05$, **$P < 0.01$, ***$P < 0.001$, ****$P < 0.0001$. All tests shown in this figure were acquired from the same cohort.

(4–8, 23). Hyperactivity in nK_{ATP}-GOF mice is consistent with findings in mouse models of attention-deficit hyperactivity disorder (ADHD) (27) and correlates with ADHD diagnoses in individuals with K_{ATP}-GOF–induced DEND (4, 28). They also mirrored the opposite effects: hypoactivity and impaired motor function observed in K_{ATP}-KO mice (15). Sensorimotor deficits in nK_{ATP}-GOF mice are consistent with clinical reports showing neuromuscular problems and developmental delay in motor milestones in individuals diagnosed with DEND (7, 23), deficits that had been ascribed to K_{ATP}-GOF expression in cerebellar Purkinje neurons in mice (10). The impairment in escape path length and latency in nK_{ATP}-GOF mice in MWM-cued trials suggests that nonassociative factors (visual/sensorimotor disturbances) affected their performance to locate and swim to the platform, which is supported by slower swimming speeds and poor sensorimotor performance, factors which may also have influenced their reduced performance on place and probe trials. Impairments in contextual fear and auditory cue conditioning in nK_{ATP}-GOF mice could arise from faster habituation relative to controls or from an inability to sustain freezing because of hyperactivity. These results are consistent with impairments to acquisition and early consolidation of contextual memory in C57BL/6J mice intrahippocampally injected with Dz (17). Strikingly, βK_{ATP}-GOF mice, with the expression of K_{ATP}-GOF channels in pancreatic β-cells, demonstrated severe diabetes but not broad neurological features, further suggesting that the neurological features of DEND arise from expression of K_{ATP}-GOF channels in the brain.

By contrast, hK_{ATP}-GOF mice did not show significant impairments on sensorimotor or rotarod tests, although they demonstrated increased locomotor activity. Slower swimming speeds in hK_{ATP}-GOF mice suggest that they may not be completely free of compromised motor function; however, the impaired retention performance in the probe trial was as strong as in nK_{ATP}-GOF mice. Indeed, since no significant spatial learning deficits were observed in the hK_{ATP}-GOF mice, we cannot conclude that poor performance on the probe trial is due to slower swimming speeds but may reflect a selective retention deficit. A specific contextual conditioning deficit in the absence of an auditory cue impairment in hK_{ATP}-GOF reinforces the hippocampal specificity and symptomatology of this model and suggests that additional findings in auditory fear conditioning in nK_{ATP}-GOF mice have an extrahippocampal origin. These results are in agreement with intellectual learning and memory deficits observed in human DEND (4–8, 23). Our studies not only parallel the cognitive deficits reported in humans carrying K_{ATP}-GOF mutations (29–31) but also underscore the role of hippocampal K_{ATP} channels in learning and memory processes.

We have provided substantial evidence here that the neuronal expression of K_{ATP}-GOF subunits leads to motor dysfunction and spatial learning and memory deficits in K_{ATP}-GOF mice. Surprisingly, somewhat similar effects were previously reported in global K_{ATP}-KO mice (17). However, the application of Glib directly into central neurons by intraseptal injection improved spontaneous alternation and memory defects induced by galanin or morphine in rats (18, 19), which suggests that the loss of K_{ATP} in nonhippocampal neurons may contribute to the learning and memory deficits in the global K_{ATP}-KO animal. In our study, impaired LTP induction in hippocampal slices from K_{ATP}-GOF mice was associated with cognitive deficits. K_{ATP} channels are present pre- and postsynaptically in CA1 hippocampal neurons (20, 32). Thus, K_{ATP}-GOF mutations may provide a barrier to LTP by persistently reducing presynaptic membrane potential and decreasing Ca^{2+} influx while postsynaptically reducing N-methyl-D-aspartate receptor (NMDAR) function by retaining Mg^{2+} channel block. The K_{ATP}-GOF mutation used here is expected to increase channel open probability and reduce ATP sensitivity but maintain maximum whole-cell K_{ATP} conductances. While dissociated hK_{ATP}-GOF neurons demonstrated no overall changes in whole-cell K_{ATP} currents, nK_{ATP}-GOF neurons showed an overall small reduction relative to control littermates. Given the very small conductances and variability in the sampled measurements, this could potentially reflect compensatory changes in channel availability, but it is consistent with the lack of any gross increase in K_{ATP} channel density driving the phenotype.

In dissociated hippocampal neurons from both nK_{ATP}-GOF and hK_{ATP}-GOF mice, sensitivity to Tol is still observed, indicating inhibition of K_{ATP} by direct pharmacological action. Homomeric expression of the same Kir6.2 N-terminal truncation in recombinant cell lines resulted in reduced sensitivity to Tol (33); however, in the present study, $Kir6.2^{[K185Q,\Delta N30]}$ mutant subunits are expressed with endogenous wild-type Kir6.2 subunits, approximating the human heterozygous condition and forming functional channels with varying Tol sensitivity as a result of variable wild-type and mutant subunit ratios. This may help to explain why neurons in a dissociated culture did not demonstrate any obvious difference in Tol sensitivity. Intraseptal injections of Glib attenuate galanin- or morphine-induced behavioral impairments in rats, suggesting a direct effect of this drug on K_{ATP} channels to modulate neural function and behavior (18, 19). Given this, the failure of Glib-treated nK_{ATP}-GOF mice to demonstrate broad improvements in sensorimotor and cognitive features is surprising but consistent with previous findings showing that systemic administration of Glib fails to achieve therapeutic levels in the brain and cerebrospinal fluid of normal rodents, even with doses 10 times higher than those used in our study (34). Improvements in some sensorimotor features in Glib-treated nK_{ATP}-GOF mice may thus reflect sulfonylurea action on K_{ATP} channels in the peripheral nervous system. These results are consistent with findings in humans treated with sulfonylureas in which the restoration of muscular tone and other sensorimotor functions is far more common than improvements in cognitive deficits (4, 7, 8, 23–25, 30, 35, 36).

These findings indicate that K_{ATP}-GOF channels in hippocampal neurons play an important role in learning and memory deficits and that the cognitive deficits in DEND result from neuronal K_{ATP}-GOF expression rather than from diabetes per se. The inefficacy of sulfonylureas in improving cognitive deficits in mice is in agreement with the limited neurological improvements observed in human DEND treatment. These studies have important clinical implications, pointing to potential mechanisms underlying cognitive deficits of K_{ATP}-induced DEND and indicating the need for novel drugs to treat neurological features arising from K_{ATP}-GOF mutations while also providing a platform to study other brain abnormalities induced by ion channel dysfunction.

Methods

Animals. Cre-inducible $Kir6.2^{[K185Q,\Delta N30]}$-GOF transgenic mice were previously generated (9) (*SI Appendix*). $Kir6.2^{[K185Q,\Delta N30]}$ mice were crossed to Syn-Cre mice (37), dopamine receptor D3-Cre (Drd3-Cre) mice [rederived "in house" (38)], or tamoxifen-inducible Pdx-CreERTx mice to generate pan-neuronal nK_{ATP}-GOF (*SI Appendix*, Fig. S1*B*), hippocampus-specific neuronal hK_{ATP}-GOF (*SI Appendix*, Fig. S1*C*), or pancreatic β-cell–specific βK_{ATP}-GOF mice, respectively (*SI Appendix*, Fig. S1*D*, induced by tamoxifen at 6 wk old) (9). Age-matched single transgenic (Syn-Cre, Drd3-Cre, Pdx1-Cre, or $Kir6.2^{[K185Q,\Delta N30]}$) and wild-type littermates were used as controls since no significant differences among genotypes were found (9). Because the mice were generated under different promoter-Cre backgrounds across studies, we have compared mutant K_{ATP}-GOF mice to their respective control littermates within a cohort. K_{ATP}-KO mice were generated by the targeted disruption of the gene encoding for the Kir6.2 subunit of the K_{ATP} channel (39). Mice were maintained on a regular chow diet and housed in a 12-h light–dark cycle. All experiments were performed in compliance with relevant laws and institutional guidelines and were approved by the Washington University Animal Studies Committee's Institutional Animal Care and Use Committee (IACUC) Protocol Approval Animal Welfare Assurance No. A-3381–01.

One-Hour Locomotor Activity and Sensorimotor Battery. Locomotor activity was evaluated as previously described (40). General activity variables (total ambulations, the number of vertical rearings) were collected along with emotionality indices (time spent, distance traveled, and entries made in central zone and distance traveled in peripheral contiguous area). The following day, mice were run on a battery of sensorimotor tests (ledge and platform; inverted screen; pole, inclined screens, and rotarod) to assay balance, strength, coordination, and movement initiation (for details, see *SI Appendix*). The averages of two trials/tests/mice were used in all analyses. The rotarod-evaluated mice during three test sessions were separated by 4 d to minimize motor learning. The rod was stationary for trial 1 and continuously rotated at constant speed (2.5 rpm) for trials 2 and 3. For trials 4 and 5, the rod rotated at an accelerating speed (0.13 rpm/s). The time an animal remained on the rod was used as the dependent variable.

MWM Navigation. Spatial learning and memory were assessed using the MWM 3 d after completion of the sensorimotor battery. A computerized tracking system (ANY-maze; Stoelting) (40, 41) recorded the swimming pathway of the mouse to the escape platform and quantified path length, latency to the escape platform, and swimming speeds during cued, place, and probe trials conducted in a pool of opaque water. Cued trials were conducted four times/day for 2 consecutive days for a total of eight trials with an intertrial interval (ITI) of 30 min and a 60 s maximum/trial, and performance was analyzed as four blocks of two trials. After 3 d, spatial learning was assessed on place condition, two blocks of two consecutive trials over 5 d with 60 s maximum/trial and an ITI of 30 s spent on platform. Blocks were separated by ∼2 h and analyzed over five blocks of four trials, each block representing 1 d of training. A 60-s probe trial was administered ∼1 h after the last place trial on day 5 when the platform was removed, and the mouse was released into the maze from the quadrant opposite where the platform was located. The amount of time the mouse spent in each quadrant of the pool and the number of times it crossed the exact location where the platform had been were recorded.

Conditioned Fear. Fear conditioning was evaluated as previously described (41) after examining spatial learning and memory. Mice were placed into one of two Plexiglas conditioning chambers (26 cm × 18 cm × 18 cm; Med-Associates), each of which contained distinct visual, tactile, and olfactory cues. Freezing behavior was assessed for a 2-min baseline period prior to tone–shock conditioning. After spending 3 min in the conditioning chamber, and every 60 s thereafter, the mice were exposed to three tone–shock pairings. Each pairing consisted of 20 s broadband white noise presented at 80 dB (conditioned stimulus; CS), with 1.0 mA continuous foot shock (unconditioned stimulus) presented during the last second of the tone. Mice were placed back into the same conditioning chamber the following day, and freezing behavior was measured over an 8-min period. After 1 d, mice were placed into a different "altered context" chamber to assay context-independent fear conditioning. Freezing behavior was recorded for a 2-min baseline period, after which mice were assessed on the auditory cue test, which involved the presentation of the tone (CS) over an 8-min period. Freezing behavior was quantified using FreezeFrame image analysis software (Actimetrics), during which freezing was defined as no movement beyond that associated with breathing. The data are presented as a percentage of time spent freezing relative to the total duration of the trial. Shock sensitivity was evaluated after fear conditioning as previously described (42).

Chronic Sulfonylurea Treatment. Glib (Glyburide) pellets at the concentration of 2.5 mg per 60-d release were obtained from Innovative Research of America. Mice that were 6-wk-old were anesthetized with Avertin © (0.25 mg/g mouse body weight), the skin on the lateral side of the neck of the animal was lifted, and pellets were implanted under the skin of the neck using a stainless-steel precision trochar (43). A total of 3 wk after pellet implantation, all mice were tested in the same behavioral suites as above (One-Hour Locomotor Activity and Sensorimotor Battery, MWM Navigation, Conditioned Fear).

LTP

Hippocampal slice preparation. Mice were collected at P30-60, anesthetized, and then their brains were harvested and transferred immediately to ice-cold sucrose-based artificial cerebrospinal fluid with 95% carbogen and prepared by vibratome (Leica VT1200) into 300-μm coronal hippocampal slices. The preparation for all solutions and specific procedures are described in *SI Appendix*.

Electrophysiology recording. All hippocampal slice experiments were performed in extracellular current-clamp mode at 30 °C and recorded using pClamp 9.2 software (Axon Instruments/Molecular Devices), digitized at 20 kHz, and filtered at 2 kHz. The fEPSPs were recorded in response to current injections (Grass Instrument-S88-stimulator) in the stimulating electrode every 20 s. After establishing maximum fEPSP amplitude with an input–output curve, current injection levels were reduced to 40% of maximum and at least 25 min of baseline recorded (see *SI Appendix* for details). After baseline, a 100-Hz tetanus stimulus was applied to the slice to induce LTP, and recording continued for at least 1 h to assess LTP induction. The slope of the rising phase (0 to 50% maximum amplitude in trace) of the fEPSP was recorded as the main determinant of changes in synaptic plasticity (see *SI Appendix* for more details).

Whole-Cell Patch Clamp Electrophysiology in Dissociated Hippocampal Neurons. Hippocampal tissue from P0-P3 experimental/control mice was dissociated and plated as a single-cell suspension onto collagen-coated tissue-culture plates. Cells were first bathed in high-sodium (identical to low-potassium solution) solution prior to local perfusion with experimental solutions (see *SI Appendix* for more details). Dz (300 μM) or Tol (500 μM) were prepared in high-potassium solution. Membrane potential was initially clamped at −70 mV and then pulsed to −120 mV for 10 ms to allow for settling. Voltage was then ramped up at a rate of 40 mV/s to a maximum of 40 mV before being stepped down again to −70 mV with voltage ramps repeated three times per condition. Currents at −120 mV (after 10-ms recovery) were measured to maximize potassium channel–mediated conductances. All recordings were performed at room temperature.

Statistical Analyses.

Mouse behavior. Data are presented as mean ± SEM. Statistical significance was determined using unpaired Student's *t* tests (asterisks). Two-way repeated-measures ANOVA (asterisks within parentheses (*)) with one between-subjects (genotype) and one within-subjects (blocks of trials) variables were used to analyze locomotor activity, rotarod, MWM, conditioned fear, LTP, and GTT data. To protect against violations of sphericity, we used the Geisser–Greenhouse method to adjust α-levels for all within-subject effects containing more than two levels. Simple effects tests were conducted following certain significant interactions and subsequent pairwise comparisons and Bonferroni correction to control for alpha inflation because of multiple comparisons (GraphPad Prism 8.4.0).

LTP electrophysiology. The slope of the rising phase of the fEPSP was calculated as the average of the maximum slope within the first 0 to 50% of the rising phase and the five preceding and five subsequent digitized samples. Slopes from successive recordings within a 3-min window were also averaged. Slopes were expressed as a percentage of baseline (calculated as the average maximum slope of the 20-min preceding LTP induction). Data were analyzed using custom MATLAB scripts (MATLAB and Statistics-Toolbox-Release-2018b, The MathWorks) and Microsoft Excel. Significance levels are denoted in each figure, and nonsignificant differences are not indicated.

Dissociated culture electrophysiology-. Current amplitudes at −120 mV (after 10 ms settling) were measured and normalized to cell capacitance. These current densities were then analyzed with two-way ANOVAs with the genotype (two levels) and the bath condition (six levels) as the between- and within-subjects factors, respectively. The Geisser–Greenhouse method was used to correct for violations of sphericity. Post-hoc pairwise Student's *t* tests comparing bath conditions (Na1 to Na1, Dz to Dz, etc.) across genotypes were performed using the Bonferroni correction to adjust for multiple comparisons. Within cells, K_{ATP} drug sensitivity was calculated as the difference in current density between Dz and Tol conditions. Differences in K_{ATP} drug sensitivities across genotypes with or without internal ATP were analyzed using unpaired two-tailed Student's *t* tests.

Data Availability. All study data are included in the article and/or *SI Appendix*.

ACKNOWLEDGMENTS. We thank Dr. Yukitoshi Izumi (Department of Psychiatry, Washington University in St. Louis) for his support on LTP experiments, Dr. Colin Nichols (Department of Cell Biology and Physiology, Washington University in St. Louis) for the useful discussion, and Ann Benz for expert technical help with hippocampal cultures. Our research was funded by NIH R01DK098584 and R01DK123163 to M.S.R. and R01MH123748 to S.M. Partial support was provided by the Intellectual–Developmental Disabilities Research Center at Washington University and National Institute of Child Health and Human Development (NICHD) U54HD087011/P50HD103425; D.F.W.

1. A. L. Gloyn *et al.*, Activating mutations in the gene encoding the ATP-sensitive potassium-channel subunit Kir6.2 and permanent neonatal diabetes. *N. Engl. J. Med.* **350**, 1838–1849 (2004).
2. M. Vaxillaire *et al.*, Kir6.2 mutations are a common cause of permanent neonatal diabetes in a large cohort of French patients. *Diabetes* **53**, 2719–2722 (2004).
3. P. Proks *et al.*, Molecular basis of Kir6.2 mutations associated with neonatal diabetes or neonatal diabetes plus neurological features. *Proc. Natl. Acad. Sci. U.S.A.* **101**, 17539–17544 (2004).
4. W. Mlynarski *et al.*, Sulfonylurea improves CNS function in a case of intermediate DEND syndrome caused by a mutation in KCNJ11. *Nat. Clin. Pract. Neurol.* **3**, 640–645 (2007).
5. K. Shimomura *et al.*, A novel mutation causing DEND syndrome: A treatable channelopathy of pancreas and brain. *Neurology* **69**, 1342–1349 (2007).
6. A. L. Gloyn *et al.*, KCNJ11 activating mutations are associated with developmental delay, epilepsy and neonatal diabetes syndrome and other neurological features. *Eur. J. Hum. Genet.* **14**, 824–830 (2006).
7. P. Bowman *et al.*, Cognitive, neurological, and behavioral features in adults with *KCNJ11* neonatal diabetes. *Diabetes Care* **42**, 215–224 (2019).
8. P. Svalastoga *et al.*, Intellectual disability in K_{ATP} channel neonatal diabetes. *Diabetes Care* **43**, 526–533 (2020).
9. M. S. Remedi *et al.*, Secondary consequences of beta cell inexcitability: Identification and prevention in a murine model of K(ATP)-induced neonatal diabetes mellitus. *Cell Metab.* **9**, 140–151 (2009).
10. R. H. Clark *et al.*, Muscle dysfunction caused by a K_{ATP} channel mutation in neonatal diabetes is neuronal in origin. *Science* **329**, 458–461 (2010).
11. A. A. Dunn-Meynell, N. E. Rawson, B. E. Levin, Distribution and phenotype of neurons containing the ATP-sensitive K^+ channel in rat brain. *Brain Res.* **814**, 41–54 (1998).
12. C. Karschin, C. Ecke, F. M. Ashcroft, A. Karschin, Overlapping distribution of K(ATP) channel-forming Kir6.2 subunit and the sulfonylurea receptor SUR1 in rodent brain. *FEBS Lett.* **401**, 59–64 (1997).
13. T. Miki, K. Nagashima, S. Seino, The structure and function of the ATP-sensitive K+ channel in insulin-secreting pancreatic beta-cells. *J. Mol. Endocrinol.* **22**, 113–123 (1999).
14. N. Zerangue, B. Schwappach, Y. N. Jan, L. Y. Jan, A new ER trafficking signal regulates the subunit stoichiometry of plasma membrane K(ATP) channels. *Neuron* **22**, 537–548 (1999).
15. R. M. Deacon *et al.*, Behavioral phenotyping of mice lacking the K ATP channel subunit Kir6.2. *Physiol. Behav.* **87**, 723–733 (2006).
16. C. Choeiri *et al.*, Cerebral glucose transporters expression and spatial learning in the K-ATP Kir6.2(-/-) knockout mice. *Behav. Brain Res.* **172**, 233–239 (2006).
17. A. Betourne *et al.*, Involvement of hippocampal CA3 K(ATP) channels in contextual memory. *Neuropharmacology* **56**, 615–625 (2009).
18. M. R. Stefani, P. E. Gold, Intra-septal injections of glucose and glibenclamide attenuate galanin-induced spontaneous alternation performance deficits in the rat. *Brain Res.* **813**, 50–56 (1998).
19. M. R. Stefani, G. M. Nicholson, P. E. Gold, ATP-sensitive potassium channel blockade enhances spontaneous alternation performance in the rat: A potential mechanism for glucose-mediated memory enhancement. *Neuroscience* **93**, 557–563 (1999).
20. D. Griesemer, C. Zawar, B. Neumcke, Cell-type specific depression of neuronal excitability in rat hippocampus by activation of ATP-sensitive potassium channels. *Eur. Biophys. J.* **31**, 467–477 (2002).
21. J. R. Martínez-François *et al.*, BAD and K_{ATP} channels regulate neuron excitability and epileptiform activity. *eLife* **7**, e32721 (2018).
22. E. R. Pearson *et al.*, Switching from insulin to oral sulfonylureas in patients with diabetes due to Kir6.2 mutations. *N. Engl. J. Med.* **355**, 467–477 (2006).
23. J. Beltrand *et al.*, Sulfonylurea therapy benefits neurological and psychomotor functions in patients with neonatal diabetes owing to potassium channel mutations. *Diabetes Care* **38**, 2033–2041 (2015).
24. J. H. Cho *et al.*, DEND syndrome with heterozygous KCNJ11 mutation successfully treated with sulfonylurea. *J. Korean Med. Sci.* **32**, 1042–1045 (2017).
25. A. S. Slingerland, R. Nuboer, M. Hadders-Algra, A. T. Hattersley, G. J. Bruining, Improved motor development and good long-term glycaemic control with sulfonylurea treatment in a patient with the syndrome of intermediate developmental delay, early-onset generalised epilepsy and neonatal diabetes associated with the V59M mutation in the KCNJ11 gene. *Diabetologia* **49**, 2559–2563 (2006).
26. C. G. Nichols, KATP channels as molecular sensors of cellular metabolism. *Nature* **440**, 470–476 (2006).
27. P. Majdak *et al.*, A new mouse model of ADHD for medication development. *Sci. Rep.* **6**, 39472 (2016).
28. K. A. Landmeier, M. Lanning, D. Carmody, S. A. W. Greeley, M. E. Msall, ADHD, learning difficulties and sleep disturbances associated with KCNJ11-related neonatal diabetes. *Pediatr. Diabetes* **18**, 518–523 (2017).
29. K. Shimomura, Y. Maejima, K_{ATP} channel mutations and neonatal diabetes. *Intern. Med.* **56**, 2387–2393 (2017).
30. T. Pipatpolkai, S. Usher, P. J. Stansfeld, F. M. Ashcroft, New insights into K_{ATP} channel gene mutations and neonatal diabetes mellitus. *Nat. Rev. Endocrinol.* **16**, 378–393 (2020).
31. K. Busiah *et al.*, Neuropsychological dysfunction and developmental defects associated with genetic changes in infants with neonatal diabetes mellitus: A prospective cohort study. *Lancet Diabetes Endocrinol.* **1**, 199–207 (2013). Correction in: *Lancet Diabetes Endocrinol.* **1**, e14 (2013).
32. N. Matsumoto, S. Komiyama, N. Akaike, Pre- and postsynaptic ATP-sensitive potassium channels during metabolic inhibition of rat hippocampal CA1 neurons. *J. Physiol.* **541**, 511–520 (2002).
33. J. C. Koster, Q. Sha, C. G. Nichols, Sulfonylurea and K(+)-channel opener sensitivity of K(ATP) channels. Functional coupling of Kir6.2 and SUR1 subunits. *J. Gen. Physiol.* **114**, 203–213 (1999).
34. C. Lahmann, H. B. Kramer, F. M. Ashcroft, Systemic administration of glibenclamide fails to achieve therapeutic levels in the brain and cerebrospinal fluid of rodents. *PLoS One* **10**, e0134476 (2015).
35. J. C. Koster *et al.*, The G53D mutation in Kir6.2 (KCNJ11) is associated with neonatal diabetes and motor dysfunction in adulthood that is improved with sulfonylurea therapy. *J. Clin. Endocrinol. Metab.* **93**, 1054–1061 (2008).
36. L. Garcin *et al.*, Neonatal diabetes due to potassium channel mutation: Response to sulfonylurea according to the genotype. *Pediatr. Diabetes* **21**, 932–941 (2020).
37. D. Rempe *et al.*, Synapsin I Cre transgene expression in male mice produces germline recombination in progeny. *Genesis* **44**, 44–49 (2006).
38. S. Gong *et al.*, Targeting Cre recombinase to specific neuron populations with bacterial artificial chromosome constructs. *J. Neurosci.* **27**, 9817–9823 (2007).
39. T. Miki *et al.*, Defective insulin secretion and enhanced insulin action in KATP channel-deficient mice. *Proc. Natl. Acad. Sci. U.S.A.* **95**, 10402–10406 (1998).
40. D. F. Wozniak *et al.*, Apoptotic neurodegeneration induced by ethanol in neonatal mice is associated with profound learning/memory deficits in juveniles followed by progressive functional recovery in adults. *Neurobiol. Dis.* **17**, 403–414 (2004).
41. L. R. Stein *et al.*, Expression of Nampt in hippocampal and cortical excitatory neurons is critical for cognitive function. *J. Neurosci.* **34**, 5800–5815 (2014).
42. S. Johnson, D. F. Wozniak, S. Imai, CA1 *Nampt* knockdown recapitulates hippocampal cognitive phenotypes in old mice which nicotinamide mononucleotide improves. *NPJ Aging Mech. Dis.* **4**, 10 (2018).
43. M. S. Remedi, C. G. Nichols, Chronic antidiabetic sulfonylureas in vivo: Reversible effects on mouse pancreatic beta-cells. *PLoS Med.* **5**, e206 (2008).
44. K. A. Yamada, S. M. Rothman, Diazoxide blocks glutamate desensitization and prolongs excitatory postsynaptic currents in rat hippocampal neurons. *J. Physiol.* **458**, 409–423 (1992).